Journal of Nuclear Materials 382 (2008) 154–159

Contents lists available at ScienceDirect

Journal of Nuclear Materials

journal homepage: www.elsevier.com/locate/jnucmat

# Microstructural evolution under high flux irradiation of dilute Fe–CuNiMnSi alloys studied by an atomic kinetic Monte Carlo model accounting for both vacancies and self interstitials

E. Vincent [a,b], C.S. Becquart [a,*], C. Domain [a,b]

[a] Laboratoire de Métallurgie Physique et Génie des Matériaux, UMR 8517, Université de Lille 1, F-59655 Villeneuve d'Ascq Cedex, France
[b] EDF-R&D Département MMC, Les Renardières, F-77818 Moret sur Loing Cedex, France

ARTICLE INFO

*PACS:*
61.72.Ji
61.80.−x
71.20.Be
71.15.Mb

ABSTRACT

Under neutron irradiation, a large amount of point defects (vacancies and interstitials) are created. In the irradiated pressure vessel steels, weakly alloyed, these point defects are responsible for the diffusion of the solute atoms, leading to the formation of solute rich precipitates within the matrix. Ab initio calculations based on the density functional theory have been performed to determine the interactions of point defects with solute atoms in dilute FeX alloys (X = Cu, Mn, Ni or Si). For Mn, the results of these calculations lead to think that solute transport in α-Fe can very likely take place through an interstitial mechanism as well as via vacancies while the other solutes (Cu, Ni and Si) which establish strong bonds with vacancies diffuse more likely via vacancies only. The database thus created has been used to parameterize an atomic kinetic Monte Carlo model taking into account both vacancies and interstitials. Some results of irradiation damage in dilute Fe–CuNiMnSi alloys obtained with this model will be presented.


## 1. Introduction

The formation of solute rich precipitates or clusters in reactor pressure vessel steels under neutron irradiation is a very intriguing phenomenon. It is now well accepted that during irradiation, a large amount of point defects (vacancies and interstitials) are created within displacement cascades. In the irradiated pressure vessel steels, weakly alloyed, these point defects are very probably responsible for the diffusion of solute atoms, leading to the formation of clusters enriched in Cu, Ni, Mn and Si [1,2]. Light can be shed on the cluster formation with the help of numerical simulations at the atomistic level, as they can help understanding the elementary mechanisms which lead to the changes observed. Among the different techniques available, Atomic kinetic Monte Carlo (AKMC) based on the diffusion of point defects is a powerful tool to simulate the microstructural kinetic evolution under irradiation. We have thus used ab initio calculations compared to experimental data to parameterize an atomic kinetic Monte Carlo model whose aim is to simulate the medium term formation of Cu–Ni–Mn–Si enriched clusters under irradiation. The energetic properties used in the fitting procedure were the solute mixing energies in Fe, different binding energies of solute (Cu, Ni, Mn, Si)-point defect complexes, migration energies and interface energies. The model was in a first step parameterized on thermal ageing experiments of alloys of growing complexity [3–5]. This first step insured that the interactions between vacancies and solute atoms were correctly modeled. In a second step, we introduced interstitials in the model. This paper describes the method used as well as some results obtained for the simulation of 'neutron' or electron irradiations of model alloys.

## 2. Methodology

### 2.1. Ab initio calculations

Our calculations have been done using the Vienna Ab initio Simulation Package VASP [6,7]. They were performed in a plane-wave basis. Exchange and correlation were described by the Perdew–Zunger functional, adding a non-local correction in the form of the generalised gradient approximation (GGA) of Perdew and Wang. All the calculations were done in the spin polarised GGA using the supercell approach with periodic boundary conditions. The ultrasoft pseudopotentials used in this work come from the VASP library. Brillouin zone (BZ) sampling was performed using the Monkhorst–Pack scheme. The defect calculations were done at constant volume, relaxing only the atomic positions in a supercell dimensioned with the equilibrium lattice parameter for Fe (2.8544 Å). The plane wave cut-off energy was 240 eV. The results were obtained using 128-atom supercells with a BZ sampling of

* Corresponding author.
*E-mail address:* charlotte.becquart@univ-lille1.fr (C.S. Becquart).

0022-3115/$ - see front matter © 2008 Elsevier B.V. All rights reserved.
doi:10.1016/j.jnucmat.2008.08.019

27 k points. More details on the method can be found in a previous work [8].

After a thorough comparison [5] of the data obtained using the Projector Augmented Wave (PAW) and the UltraSoft PseudoPotential (USPP) formalisms, USPP was chosen. The PAW method should theoretically give better results than the USPP one for 3d-transition metals as it gives a better description of the core electrons. This method gives indeed better results as far as the magnetic moments are concerned but appears to be less appropriate for the energies needed to parameterize our model.

### 2.2. Monte Carlo model

The Monte Carlo code, LAKIMOCA, developed at Electricité de France (EDF) [9], has been improved to treat complex alloys (Fe–CuNiMnSi) as well as interstitials which play a non negligible role in the embrittlement of RPV steels under irradiation. The motive for introducing interstitials in the vacancy AKMC was two fold. First of all, interstitials move very quickly and can recombine with vacancies, decreasing the amount of vacancies available for diffusion. Second of all, our ab initio results indicate that Mn is very likely to be able to diffuse via some mechanisms involving interstitials [10] as well as vacancies, while the other solutes (Cu, Ni and Si) which establish strong bonds with vacancies are more likely to diffuse via vacancies only [11].

The model is based on the residence time algorithm [12]. Both vacancy and interstitial diffusions are determined by the calculation of the probabilities to jump to a first nearest neighbour site. This probability is obtained as follows:

$$\Gamma_{X,V} = \nu_X \exp\left(-\frac{E_a}{kT}\right), \tag{1}$$

where $\nu_X$ is the attempt frequency, equal to $6 \times 10^{12}\ s^{-1}$, and $E_a$ is the activation energy of the jump.

The activation energy $E_a$ is obtained using an environment-dependent model, which satisfies the detailed balance rule:

$$E_a = E_{a_0} + \frac{E_f - E_i}{2} \tag{2}$$

where $E_i$ and $E_f$ are the system energies, respectively, before and after the jump of the vacancy or of the interstitial. Recombination between an interstitial and a vacancy takes place as soon as they become second nearest neighbors.

For vacancy jumps $E_i$ and $E_f$ are determined using pair interactions, according to the following equation:

$$E = \sum_{i=1,2} \sum_{j<k} \varepsilon^{(i)}(S_j - S_k) \tag{3}$$

where $i$ equals 1 or 2 and corresponds respectively to first or second nearest neighbor interaction, $j$ and $k$ to the lattice site and $S_j$ (resp. $S_k$) is the species occupying site $j$ (resp. $k$): $S_j$ in {Fe, V, X} where X = Cu, Ni, Mn or Si. In the calculation of the activation energy for a vacancy jump, the interactions due to interstitials are not taken into account. For interstitial jumps, $E_i$ and $E_f$ are determined using (3) and adding to it the contribution of the dumbbells.

#### 2.2.1. Activation energy in the case of a vacancy jump

The reference activation energy $E_{a_0}$ in Eq. (2) depends only on the type of the migrating atom: it is the ab initio vacancy migration energy in pure Fe when the vacancy jumps towards an Fe atom and the ab initio solute migration energy in pure Fe when the vacancy jumps towards a solute atom. The pair interactions, necessary to determine $E_i$ and $E_f$, have been obtained from the following set of equations:

$$E_{coh}(X) = 4\varepsilon^{(1)}_{(X-X)} + 3\varepsilon^{(2)}_{(X-X)} \tag{4}$$

$$E_{mix}(X \to Fe) = -4\varepsilon^{(1)}_{(Fe-Fe)} - 3\varepsilon^{(2)}_{(Fe-Fe)} + 8\varepsilon^{(1)}_{(Fe-X)} + 6\varepsilon^{(2)}_{(Fe-X)} - 4\varepsilon^{(1)}_{(X-X)} - 3\varepsilon^{(2)}_{(X-X)} \tag{5}$$

$$E_{int(100)}(Fe/X) = -2\varepsilon^{(1)}_{(Fe-Fe)} - \varepsilon^{(2)}_{(Fe-Fe)} + 4\varepsilon^{(1)}_{(Fe-X)} + 2\varepsilon^{(2)}_{(Fe-X)} - 2\varepsilon^{(1)}_{(X-X)} - \varepsilon^{(2)}_{(X-X)} \tag{6}$$

$$E_b^{(1)}(V-X) = \varepsilon^{(1)}_{(Fe-X)} + \varepsilon^{(1)}_{(Fe-V)} - \varepsilon^{(1)}_{(Fe-Fe)} - \varepsilon^{(1)}_{(V-X)} \tag{7}$$

$$E_{for}(V^X) = 8\varepsilon^{(1)}_{(X-V)} + 6\varepsilon^{(2)}_{(X-V)} - 4\varepsilon^{(1)}_{(X-X)} - 3\varepsilon^{(2)}_{(X-X)} \tag{8}$$

$$E_b^{(i)}(V-V) = 2\varepsilon^{(i)}_{(Fe-V)} - \varepsilon^{(i)}_{(Fe-Fe)} - \varepsilon^{(i)}_{(V-V)} \tag{9}$$

$$E_b^{(i)}(X-Y) = \varepsilon^{(i)}_{(Fe-X)} + \varepsilon^{(i)}_{(Fe-Y)} - \varepsilon^{(i)}_{(Fe-Fe)} - \varepsilon^{(i)}_{(X-Y)} \tag{10}$$

$$\varepsilon^{(2)}_{(Fe-Fe)} = \alpha\varepsilon^{(1)}_{(Fe-Fe)} \tag{11}$$

$$\varepsilon^{(2)}_{(Fe-V)} = \beta\varepsilon^{(1)}_{(Fe-V)} \tag{12}$$

$$\varepsilon^{(2)}_{(X-X)} = \lambda_X\varepsilon^{(2)}_{(Fe-Fe)} \tag{13}$$

where $E_{coh}(X)$ is the cohesive energy of solute $X$ in the body centered cubic (bcc) structure, $E_{mix}$ ($X \to Fe$) the mixing energy, $E_{int(100)}$ ($Fe/X$) the interface energy along the (1 0 0) plane and $E_b$ binding energies. Moreover, $i$ equals 1 or 2 and stands for first or second nearest neighbor respectively; $\alpha$ and $\beta$ are constants, $\lambda_X$ is a solute depending constant and $X$, $Y$ are solute atoms. The energies used in the set of equations have been determined using ab initio calculations [4,10,11,13]. Ab initio calculations do have limitations and uncertainties; thus the ab initio values were examined with a critical eye. The energies calculated have been compared to experiments or thermodynamical data, when that was possible, and sometimes readjusted accordingly. This adjustment was made by simulating age hardening of binaries, then ternaries then more complicated alloys and comparing the results obtained with experimental results. A detailed description of the parameterization of the FeCu system can be found in [14]. During this procedure some of the values obtained ab initio used in Eqs. (4)–(10) had to be slightly modified so as to obtain a set of values more in agreement with experiments and phase diagrams as well as with other ab initio data. The energy difference between the original ab initio data and the adjusted data is less than 0.1 eV which corresponds to the ab initio uncertainty. Two examples of the kind of changes done follow. First, Mn–Cu binding energies were increased in order to better reproduce precipitation in a Fe–CuMnSi alloy aged at 550 °C [15]. With the ab initio values ($E_b^{(1)}$ (Cu–Mn) = 0.02 eV; $E_b^{(2)}$ (Cu–Mn) = –0.07 eV), the precipitates formed were composed of less than 1 at.% of Mn atoms instead of 8.1 at.% as measured experimentally. After some energy adjustments ($E_b^{(1)}$ (Cu–Mn) = 0.05 eV; $E_b^{(2)}$ (Cu–Mn) = 0.03 eV), the Cu precipitates contained 10 at.% of Mn atoms. Second, the Fe/Mn interface energy along the (100) plane was slightly increased, keeping its negative sign. This change was done in order to agree more with the experimental fact that FeMn is an ideal solution. Indeed, using the AKMC model with the ab initio value ($E_{int(100)}$ (Fe/Mn) = –177 mJ m$^{-2}$), when, for instance, 1.5 at.% Mn atoms were randomly introduced in a simulation box of α-Fe, a great part (around 75%) of the Mn atoms, which were bound to

**Table 1**
Properties chosen to parameterize each binary system FeX (X = Cu, Mn, Ni et Si)

| Property | FeCu | FeMn | FeNi | FeSi |
|---|---|---|---|---|
| $E_{coh}$ ($X$) (eV) | −3.49 | −2.92 | −4.34 | −4.03 |
| $E_{sol}$ ($X \to Fe$) (eV) | 0.50 | −0.16 | −0.17 | −1.09 |
| $E_{int(100)}$ ($Fe/X$) (mJ m$^{-2}$) | 407 | −116 | −194 | −969 |
| $E_{for}$ ($V^X$) (eV) | 1.6 | 1.4 | 1.48 | −0.21 |
| $E_b^{(1)}$ (V–X) (eV) | 0.07 | 0.04 | 0.01 | 0.11 |

Cohesive energies of the pure solute: $E_{coh.}$, solution energies of the solute in Fe: $E_{sol.}$, interface energies between Fe and the solute along (100): $E_{int(100).}$ vacancy formation energies in the solute: $E_{for}$ and binding energies between the solute atom and a vacancy in an Fe matrix: $E_b$.

**Table 2**
Binding energies used in the parameterization of complex alloys

| Property | Mn | Ni | Cu |
|---|---|---|---|
| $E_b^{(1)}$ (Si–X) (eV) | −0.03 | 0.00 | 0.06 |
| $E_b^{(2)}$ (Si–X) (eV) | −0.36 | −0.12 | −0.05 |
| $E_b^{(1)}$ (Mn–X) (eV) | | −0.12 | 0.05 |
| $E_b^{(2)}$ (Mn–X) (eV) | | −0.12 | 0.03 |
| $E_b^{(1)}$ (Ni–X) (eV) | | | 0.02 |
| $E_b^{(2)}$ (Ni–X) (eV) | | | 0.02 |

1 nn stands for first nearest neighbor, 2 nn for second nearest neighbor.

other Mn atoms in the initial random distribution became isolated. With the adjusted value ($E_{\text{int}\langle 100\rangle}$(Fe/Mn) = −116 mJ m$^{-2}$), there was almost no change of the initial random microstructure, which indicates that the solution is indeed ideal. One difficult problem faced in the work presented here is that the binding energy absolute values are low and often within the calculation uncertainty. Consequently, even if in the course of the parameterization, their sign changes as in the case of the Mn-Cu second nearest neighbor binding energy ($E_b^{(2)}$ (Cu–Mn) = −0.07 eV was replaced by $E_b^{(2)}$ (Cu–Mn) = 0.03 eV), the modification is not so drastic and usually remains within the calculation uncertainty. Furthermore, Mn is a difficult element to model as its magnetic state appears to be very dependent on the calculations. The final values for the properties used to get the interaction parameters are given in Tables 1 and 2. The resulting interaction parameters are presented in Table 3.

### 2.2.2. Activation energy in the case of an interstitial jump

Previous calculations [10] indicate that even when a solute lies in the vicinity of a dumbbell, the dumbbell remains oriented along the ⟨1 1 0⟩ direction. Thus, only ⟨1 1 0⟩ dumbbells are treated in the Monte Carlo code. Eight possible jumps exist for these dumbbells [16,17]. In this work, only the most probable jump of a pure iron dumbbell in α-Fe, i.e. the translation-60° rotation jump of a dumbbell to a first nearest neighbor [10] is taken into account (see Fig. 1).

The total energy of the system for the jump of a ⟨1 1 0⟩ dumbbell is obtained by adding to Eq. (3) an energy term $E_{\text{dumb}}$ due to the presence of $N_{\text{dumb}}$ dumbbells. We used the fact that the binding energy of a cluster containing a dumbbell and many solute atoms can be obtained as a sum of binding energies between entities taken two by two [5] to decompose $E_{\text{dumb}}$ in different contributions as follows:

$$E_{\text{dumb}} = N_{\text{dumb}}E_{\text{for}}^{\langle 110\rangle} + \sum_{\text{dumb}_i}\left(\sum_j E_b^{1\text{nnComp}}(X^{\text{dumb}_i} - X_j^{1\text{nncomp}}) + \sum_j E_b^{1\text{nnTens}}(\text{dumb}_{\text{Fe-Fe}} - X_j^{1\text{nntens}})E_b^{\text{mixed}}(X^{\text{dumb}_i} - Y^{\text{dumb}_i}) + \sum_{j<i} E_b(\text{dumb}_i - \text{dumb}_j)\right) \quad (14)$$

**Table 3**
Optimized pair interactions for the Fe–CuNiMnSi complex alloys (eV)

| | | | | | | |
|---|---|---|---|---|---|---|
| $\varepsilon^{(1)}_{(\text{Fe-Fe})}$ | −0.611 | $\varepsilon^{(2)}_{(Si-Si)}$ | −0.611 | $\varepsilon^{(1)}_{(vac-\text{Cu})}$ | −0.102 | $\varepsilon^{(1)}_{(\text{Cu-Mn})}$ | −0.365 |
| $\varepsilon^{(2)}_{(\text{Fe-Fe})}$ | −0.611 | $\varepsilon^{(1)}_{(\text{Fe}-vac)}$ | −0.163 | $\varepsilon^{(2)}_{(vac-\text{Cu})}$ | −0.180 | $\varepsilon^{(2)}_{(\text{Cu-Mn})}$ | −0.621 |
| $\varepsilon^{(1)}_{(vac-vac)}$ | 0.126 | $\varepsilon^{(2)}_{(\text{Fe}-vac)}$ | −0.163 | $\varepsilon^{(1)}_{(vac-\text{Ni})}$ | −0.213 | $\varepsilon^{(1)}_{(\text{Cu}-Si)}$ | −0.611 |
| $\varepsilon^{(2)}_{(vac-vac)}$ | −0.014 | $\varepsilon^{(1)}_{(\text{Fe-Cu})}$ | −0.480 | $\varepsilon^{(2)}_{(vac-\text{Ni})}$ | −0.193 | $\varepsilon^{(2)}_{(\text{Cu}-Si)}$ | −0.566 |
| $\varepsilon^{(1)}_{(\text{Cu-Cu})}$ | −0.414 | $\varepsilon^{(2)}_{(\text{Fe-Cu})}$ | −0.571 | $\varepsilon^{(1)}_{(vac-\text{Mn})}$ | −0.038 | $\varepsilon^{(1)}_{(\text{Ni-Mn})}$ | −0.366 |
| $\varepsilon^{(2)}_{(\text{Cu-Cu})}$ | −0.611 | $\varepsilon^{(1)}_{(\text{Fe-Ni})}$ | −0.651 | $\varepsilon^{(2)}_{(vac-\text{Mn})}$ | −0.203 | $\varepsilon^{(2)}_{(\text{Ni-Mn})}$ | −0.496 |
| $\varepsilon^{(1)}_{(\text{Ni-Ni})}$ | −0.626 | $\varepsilon^{(2)}_{(\text{Fe-Ni})}$ | −0.596 | $\varepsilon^{(1)}_{(vac-Si)}$ | −0.344 | $\varepsilon^{(1)}_{(\text{Ni}-Si)}$ | −0.723 |
| $\varepsilon^{(2)}_{(\text{Ni-Ni})}$ | −0.611 | $\varepsilon^{(1)}_{(\text{Fe-Mn})}$ | −0.446 | $\varepsilon^{(2)}_{(vac-Si)}$ | −0.248 | $\varepsilon^{(2)}_{(\text{Ni}-Si)}$ | −0.521 |
| $\varepsilon^{(1)}_{(\text{Mn-Mn})}$ | −0.271 | $\varepsilon^{(2)}_{(\text{Fe-Mn})}$ | −0.631 | $\varepsilon^{(1)}_{(\text{Cu-Ni})}$ | −0.540 | $\varepsilon^{(1)}_{(\text{Mn}-Si)}$ | −0.488 |
| $\varepsilon^{(2)}_{(\text{Mn-Mn})}$ | −0.611 | $\varepsilon^{(1)}_{(\text{Fe}-Si)}$ | −0.683 | $\varepsilon^{(2)}_{(\text{Cu-Ni})}$ | −0.576 | $\varepsilon^{(2)}_{(\text{Mn}-Si)}$ | −0.316 |

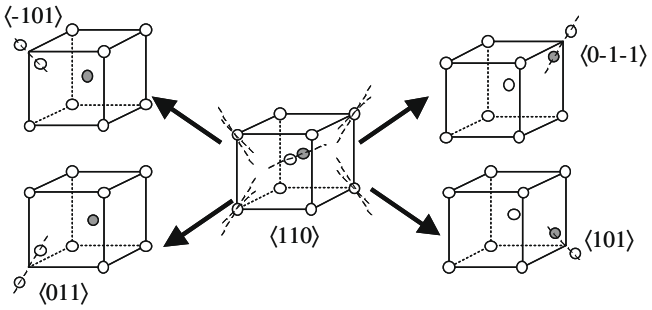


**Fig. 1.** Description of four of the eight possible jumps for a <1 1 0> dumbbell.

where $X_i$, $X_j$ et $X_k$ can be Fe, Cu, Mn, Ni or Si. $E_{\text{for}}^{\langle 110\rangle}$ is the ⟨1 1 0⟩ dumbbell formation energy in pure Fe. The meaning of the terms in Eq. (14) is represented in Fig. 2.

The interactions between two dumbbells $E_b$*(dumb–dumb)* are taken into account until the 2nd nearest neighbors and are considered identical whatever the dumbbell types, their orientation and their separation distance. The interaction value is 0.72 eV after the ab initio results of Fu et al. [18]. With this model for interstitials, interstitial clusters of size lower or equal to six are mobile.

Note that the calculation of the energy due to the dumbbell is more precise than what was done in our previous model [4]. In the calculation of $E_{\text{dumb}}$ the raw ab initio data were used (Tables 4 and 5), no adjustments were made and the simulations described in the following paragraph can thus be considered as a first test of this new model.

## 3. Results

Monte Carlo simulations of 'neutron' and electron irradiations were performed on different alloys. A rigid bcc lattice of 100 unit cells in each of the three space directions with periodic boundary conditions along the *x* and *y* axes and absorbing surfaces along *z* was used. A 'neutron' irradiation is simulated by introducing Frenkel pairs and cascade debris chosen at random in the database provided by Roger Stoller [19]. Very high fluxes as compared to the fluxes in nuclear reactors have been used in order to obtain results quickly and test the model. The choice of the alloy compositions was guided by the data available in the literature. The program generates outputs after a given number of KMC steps. For this reason, when comparing alloys, the doses are not always exactly the same for both alloys. The contribution of a Frenkel Pair to the dpa is 1, while that of a cascade debris initiated by a primary knock-on atom of energy $E_{\text{PKA}}$ is $0.8E_{\text{PKA}}/2E_{\text{D}}$, where $E_{\text{D}}$ is the threshold displacement energy (40 eV in Fe). The increment in the dose depends thus on the amount and on the energy of the displacement cascade debris introduced. For this reason, the instantaneous flux can vary from one snapshot to another, especially at the beginning of the simulations.

### 3.1. 'Neutron' irradiation of a complex alloy

Fig. 3 represents the microstructure obtained after 'neutron' irradiating a complex Fe–0.2Cu–0.53Ni–1.26Mn–0.63Si (at.%) at 300 °C. The flux was $6.5 \cdot 10^{-5}$ dpa s$^{-1}$, the dose reached at this point is $1.3 \cdot 10^{-3}$ dpa. Small vacancy solute complexes as well as interstitial solute complexes formed during the course of the irradiation as can be seen in Fig. 3. These results seem to indicate that point defect clusters act as nuclei for the formation of solute complexes.

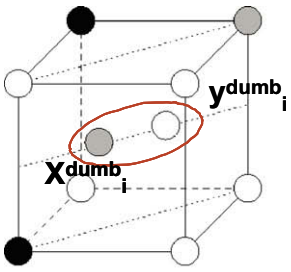


$E_b^{mixed}(X^{dumb_i} - Y^{dumb_i})$

*Binding energy of a mixed dumbbell (Tables 4 and 5)*

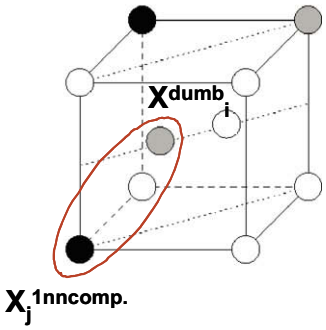


$E_b^{1nnComp}(X^{dumb_i} - X_j^{1nncomp.})$

*Binding energy of the dumbbell with an atom positioned in the plane containing the dumbbell (compressive position). The type of the dumbbell atom the closest to the atom in the matrix is taken into account (see Tables 4 and 5)*

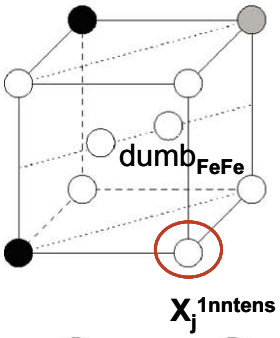


$E_b^{1nnTens}(X_j^{1nntens.} - dumb_{FeFe})$

*Binding energy of the dumbbell with an atom positioned in the plane perpendicular to the dumbbell (tensile position).The dumbbell is considered as being a pure Fe dumbbell, only the type of solute in the tensile position is taken into account. (Table 4 : 3rd line)*

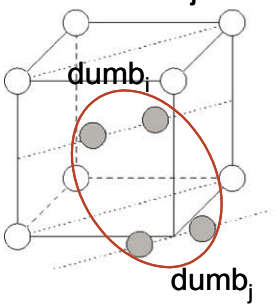


$E_b(dumb_i - dumb_j)$

*Binding energy between two dumbbells. The interactions are considered identical whatever the dumbbell types, their orientation and their separation distance. The interaction value is 0.72 eV after the ab initio results of Fu et al. [18].*

**Fig. 2.** Schematic description of the interaction terms taken into account in the activation energy determination when the moving object is a dumbbell.

**Table 4**
Binding energies (eV) for the interactions between mixed dumbbells and solute atoms when the dumbbell contains only one type of solute

| X | Cu | Mn | Ni | Si |
|---|---|---|---|---|
| $E_b^{mixed}(X^{dumb_i} - Fe^{dumb})$ | −0.46 | 0.37*af* | −0.36 | 0.01 |
| $E_b^{mixed}(X^{dumb_i} - X^{dumb_i})$ | −0.36 | 0.47*af* | −0.30 | −0.40 |
| $E_b^{1nnTens}(X^{1nntens} - dumb_{FeFe})$ | 0.07 | −0.36*f* | −0.13 | −0.23 |
| $E_b^{1nnComp}(Fe^{dumb_i} - X^{1nncomp})$ | −0.01 | 0.10*af* | −0.06 | 0.27 |
| $E_b^{1nnComp}(X^{dumb_i} - X^{1nncomp})$ | −0.18 | 0.29*af* | −0.32 | −0.50 |

The Mn magnetic state is either ferromagnetic (*f*) or antiferro-magnetic (*af*).

### 3.2. Effect of Mn on the precipitation of Cu

To investigate the influence of Mn on the precipitation of Cu under irradiation, an Fe-0.9 wt.% Cu and an Fe-0.9 wt.% Cu-1.0 wt.% s Mn were 'neutron' irradiated at 300 °C with a flux of 0.5–1.0 · $10^{-5}$ dpa $s^{-1}$ to a dose of 1.6–1.7 · $10^{-3}$ dpa. In the Mn alloy the number of clusters formed during the irradiation is higher than

**Table 5**
Binding energies (en eV) for the interactions between mixed dumbbells and solute atoms, when the dumbbell contains two different solute atoms

| X; Y | $E_b^{mixed}$ $(X^{dumb_i} - Y^{dumb_i})$ | $E_b^{1nnComp}$ $(Y^{dumb_i} - X^{1nncomp})$ | $E_b^{1nnComp}$ $(X^{dumb_i} - Y^{1nncomp})$ |
|---|---|---|---|
| Cu; Mn | −0.11 | 0.28 | −0.46 |
| Cu; Ni | −0.50 | −0.21 | −0.35 |
| Cu; Si | −0.12 | 0.04 | −0.06 |
| Mn; Ni | 0.08 | −0.30 | 0.28 |
| Mn; Si | 0.15 | −0.22 | 0.43 |
| Ni; Si | 0.05 | 0.05 | 0.11 |

For these configurations, Mn is always in an antiferro-magnetic state.

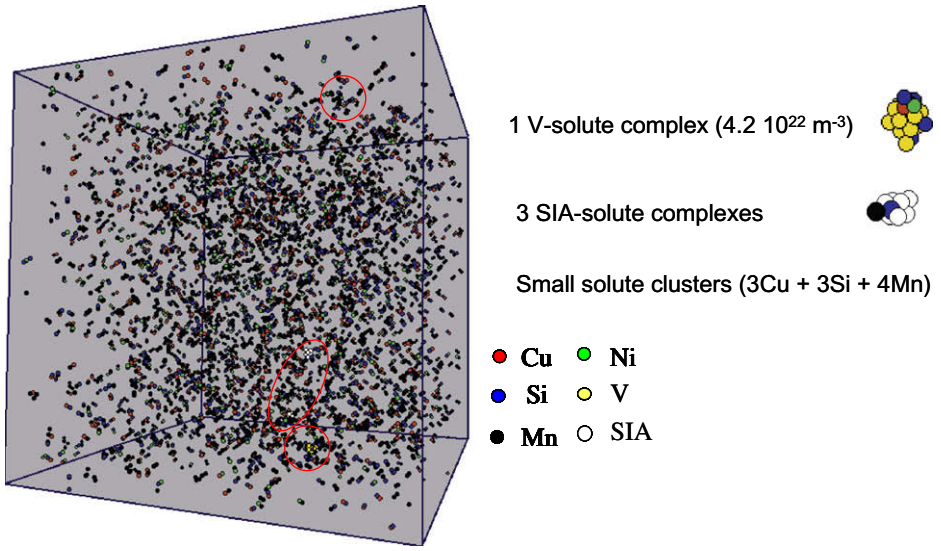


**Fig. 3.** 'Neutron' irradiation of a complex alloy: Fe–0.2Cu–0.53Ni–1.26Mn–0.63Si (at.%) at 300 °C. Flux: $6.5 \cdot 10^{-5}$ dpa $s^{-1}$ Dose: $1.3 \cdot 10^{-3}$ dpa.

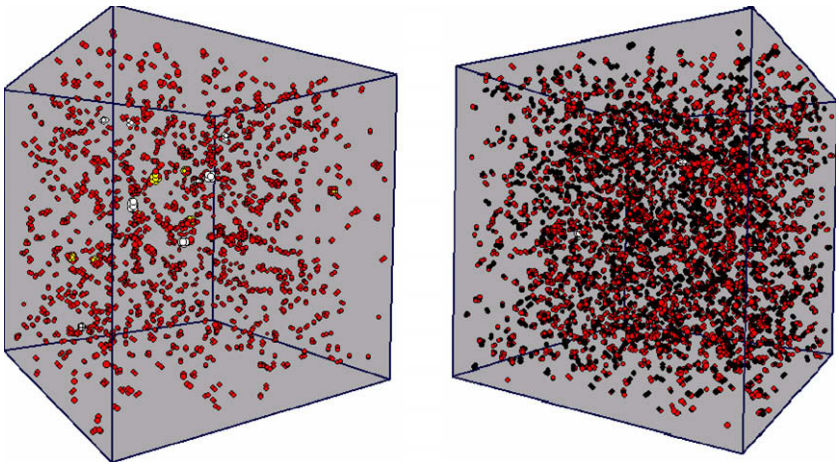

*Fe-0.9 wt% Cu*
*Flux: 1.0 $10^{-5}$ dpa $s^{-1}$*
*Dose: 1.7 $10^{-3}$ dpa*

*Fe-0.9 wt% Cu-1.0wt % Mn*
*Flux: 0.5 $10^{-5}$ dpa $s^{-1}$*
*Dose 1.6 $10^{-3}$ dpa*

**Fig. 4.** 'Neutron' irradiation at 300 °C. The microstructures show only the remaining point defects and the solute atoms involved in clusters. Cu atoms are red, Mn black, vacancies yellow and Fe interstitials white. (For interpretation of the references to colour in this figure legend, the reader is referred to the web version of this article.)

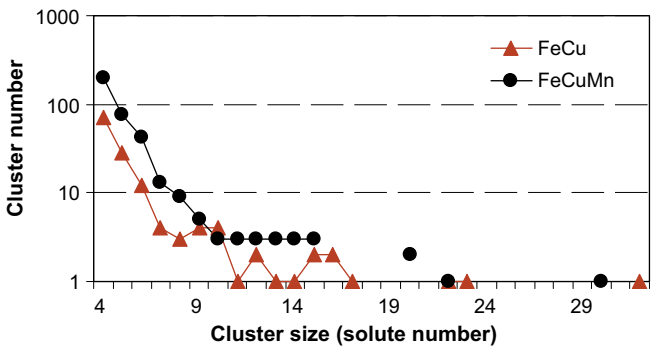


**Fig. 5.** Cluster size distribution for an Fe–0.9 wt.% Cu and an Fe-0.9 wt.% Cu-1.0 wt.% Mn 'neutron' irradiated at 300 °C.

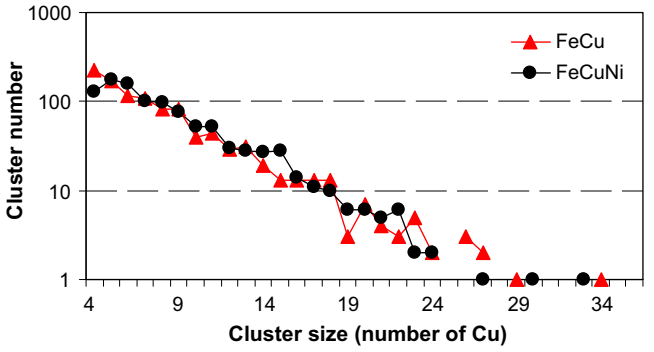


**Fig. 6.** Cluster size distribution for an Fe-1.34 at.% Cu and an Fe-1.4 at%. Cu-1.4 at.% Ni 'electron' irradiated at 300 °C.

that formed in the alloy containing no Mn, as can be seen in Figs. 4 and 5. Experimentally, the results of Glade [20] indicate that Mn seems to slow down Cu precipitation, as the clusters formed in the ternary alloy are smaller but more numerous than in the FeCu alloy. Our results, even though the length of the simulations were too short to obtain clusters with sizes comparable to the experimentally observed clusters, are thus in good agreement with the trends of these experiments.

*3.2.1. Influence of Ni on the precipitation of Cu during an electron irradiation*

An Fe-1.34 at.% Cu alloy and an Fe-1.4 at.% Cu-1.4 at.% Ni were electron irradiated at 300 °C with a flux of $5 \cdot 10^{-8}$ dpa $s^{-1}$ to a dose of 1 and $1.2 \cdot 10^{-3}$ dpa. The simulation results showed that in agreement with experiments [21,22], the presence of Ni did not change the precipitation of Cu, the amount of clusters being the same in both cases as can be seen in Fig. 6.

## 4. Conclusion

The Monte Carlo code LAKIMOCA has been improved to treat the evolution of complex alloys under irradiation due to solute diffusion via vacancy and interstitial mechanisms. The first results of microstructure evolution under Frenkel pair and cascade debris fluxes have been presented. The observed tendencies are consistent with experimental results.

## Acknowledgements

This work has been performed within the European PERFECT project (FI6O-CT-2003-508840) which has sponsored this study. This research has been done using the CRI supercomputer of the USTL supported by the Fonds Européens de Développement Régional, as well as the CEA CCRT supercomputers in the framework of an EDF-CEA contract.

## References

[1] J.T. Buswell, W.J. Phythian, R.J. McElroy, S. Dumbill, P.H.N. Ray, J. Mace, R.N. Sinclair, J. Nucl. Mater. 225 (1995) 196.
[2] P. Auger, P. Pareige, S. Welzel, J.-C. Van Duysen, J. Nucl. Mater. 280 (2000) 331.
[3] E. Vincent, C.S. Becquart, C. Domain, J. Nucl. Mater. 351 (2006) 88.
[4] E. Vincent, C.S. Becquart, C. Domain, Nucl. Instrum. and Meth. Phys. Res. B 255 (2007) 78.
[5] E. Vincent, PhD Thesis, Université de Lille, 2006.
[6] G. Kresse, J. Hafner, Phys. Rev. B 47 (1993) 558;
G. Kresse, J. Hafner, Phys. Rev. B 49 (1994) 14251.
[7] G. Kresse, J. Furthmüller, Comput. Mater. Sci. 6 (1996) 15.
[8] C. Domain, C.S. Becquart, Phys. Rev. B 65 (2002) 024103.
[9] C. Domain, C.S. Becquart, J.C. Van Duysen, Mater. Res. Soc. Symp. Proc. 650 (2001) R3.25.1.
[10] E. Vincent, C.S. Becquart, C. Domain, J. Nucl. Mater. 359 (2006) 227.
[11] E. Vincent, C.S. Becquart, C. Domain, Nucl. Instrum. and Meth. Phys. Res. B 228 (2005) 137.
[12] W.M. Young, E.W. Elcock, Proc. Phys. Soc. 89 (1966) 735.
[13] C.S. Becquart, C. Domain, Nucl. Instrum. and Meth. Phys. Res. 202 (2003) 44.
[14] E. Vincent, C.S. Becquart, C. Pareige, P. Pareige, C. Domain, J. Nucl. Mater. 373 (2008) 387.
[15] N. Maruyama, M. Sugiyama, T. Hara, H. Tamehiro, Mater. Trans. JIM 40 (1999) 268.
[16] P. Ehrhart, K.H. Robrock, H.R. Schober, in: R.A. Johnson, A.N. Orlov (Eds.), Part 1 of volume 13: physics of radiation effects in crystals, in: V.M. Agranovich, A.A. Maradudin (Eds.), Modern Problems in Condensed Matter Sciences, North Holland, Amsterdam, Oxford, New York, Tokyo, 1986.
[17] J.L. Bocquet, Philos. Mag. A 63 (1991) 157.
[18] C.-C. Fu, F. Willaime, P. Ordejón, Phys. Rev. Lett. 92 (2004) 175503.
[19] R. Stoller, J. Nucl. Mater. 276 (2000) 22.
[20] S.C. Glade, B.D. Wirth, G.R. Odette, P. Asoka-Kumar, P.A. Sterne, R.H. Howell, Philos. Mag. 85 (2005) 629.
[21] F. Maury, N. Lorenzelli, C.H. de Novion, J. Nucl. Mater. 183 (1991) 217.
[22] M.H. Mathon, PhD Thesis, Université de Parix XI, 1994.